Molecular Therapy
Nucleic Acids
Original Article

Exosomal MicroRNA-9-3p Secreted from BMSCs Downregulates ESM1 to Suppress the Development of Bladder Cancer

Hongzhou Cai,[1,6] Xuejian Yang,[2,6] Yang Gao,[3,6] Zicheng Xu,[1] Bin Yu,[1] Ting Xu,[1] Xiao Li,[1] Weizhang Xu,[1] Xinwei Wang,[4] and Lixin Hua[5]

[1]Department of Urology, The Affiliated Cancer Hospital of Nanjing Medical University & Jiangsu Cancer Hospital & Jiangsu Institute of Cancer Research, Nanjing 210009, P.R. China; [2]Department of Urology, Suqian First Hospital, Suqian 223800, P.R. China; [3]Department of Radiology, The Affiliated Cancer Hospital of Nanjing Medical University & Jiangsu Cancer Hospital & Jiangsu Institute of Cancer Research, Nanjing 210009, P.R. China; [4]Department of Oncology, The Affiliated Cancer Hospital of Nanjing Medical University & Jiangsu Cancer Hospital & Jiangsu Institute of Cancer Research, Nanjing 210009, P.R. China; [5]Department of Urology, The First Affiliated Hospital of Nanjing Medical University, Nanjing 210029, P.R. China

Exosomes, carriers to transfer endogenous molecules, derived from bone marrow-derived mesenchymal stem cells (BMSCs) have been reported to play a role in the progression of bladder cancer. Here we aimed to test the functional mechanism of microRNA-9-3p (miR-9-3p)-containing exosomes derived from BMSCs in bladder cancer. BMSCs were cocultured with bladder cancer cells, and exosomes secreted from BMSCs were identified. Next, the expression of miR-9-3p and endothelial cell-specific molecule 1 (ESM1) in bladder cancer tissues and cells was determined. Then effects of miR-9-3p and ESM1 via BMSC-derived exosomes on bladder cancer cell viability, migration, invasion, and apoptosis were determined by loss- and gain-of-function experiments and on *in vivo* tumor growth, and metastasis was assessed in nude mice. miR-9-3p expression was decreased and ESM1 was increased in bladder cancer. BMSCs inhibited bladder cancer cell viability, migration, and invasion, and induced apoptosis, whereas the addition of exosome secretion inhibitor GW4869 achieved the opposite effects. Moreover, exosomal miR-9-3p upregulation or ESM1 silencing suppressed bladder cancer cell viability, migration, and invasion; induced cell apoptosis; and inhibited *in vivo* tumor growth and metastasis. Taken together, BMSC-derived exosomal miR-9-3p suppressed the progression of bladder cancer through ESM1 downregulation, offering a potential novel therapeutic target for bladder cancer therapy.

INTRODUCTION

Bladder cancer is one of the most frequent human cancers developed via papillary and nonpapillary tracks corresponding to different clinical forms.[1] Recent estimates indicate that 80,470 new bladder cancer cases are diagnosed annually, accounting for 17,670 deaths worldwide in 2019.[2] Good outcomes of bladder cancer patients rely on early awareness of hematuria, early diagnosis, personalized therapeutic intervention, and follow-up.[3] Recently, a comprehensive genomic analysis based on data from The Cancer Genome Atlas (TCGA) database confirmed that multiple subtypes of bladder cancers are induced by different genetic changes.[4] Importantly, changes in expression of mRNAs, long non-coding RNAs (lncRNAs), and microRNAs (miRNAs) are associated with changes in epithelial-mesenchymal transition (EMT) status, carcinoma scores, histologic characteristics, and survival in bladder cancers.[5] Therefore, it is important to understand molecular changes in bladder cancer to improve both diagnosis and treatment.

Endothelial cell-specific molecule 1 (ESM1), also known as endocan, has angiogenic and inflammatory properties that may affect vascular permeability.[6] Interestingly, ESM1 is found to be highly expressed in blood vessels from invasive bladder cancer tissues.[7] Additionally, serum and urinary ESM1 levels in bladder cancer patients are higher than that of healthy subjects.[8] However, how ESM1 is involved in bladder cancer development remains unclear.

miRNAs, small non-coding RNAs, suppress translational expression and stability of mRNAs, and also control cellular processes such as cell-cycle regulation, cellular differentiation, and apoptosis. Dysregulation of miRNAs has been shown to play an essential role in the development and progression of cancers.[9] Several anti-oncologic miRNAs such as miR-145, miR-143, and miR-125b are downregulated in bladder cancer, whereas some oncogenic miRNAs such as

Received 22 April 2019; accepted 20 September 2019;
https://doi.org/10.1016/j.omtn.2019.09.023.

[6]These authors contributed equally to this work.

Correspondence: Xinwei Wang, Department of Oncology, The Affiliated Cancer Hospital of Nanjing Medical University & Jiangsu Cancer Hospital & Jiangsu Institute of Cancer Research, No. 42, Baizi Ting, Nanjing 210009, Jiangsu Province, P.R. China.
E-mail: wxwswy@163.com
Correspondence: Lixin Hua, Department of Urology, The First Affiliated Hospital of Nanjing Medical University, No. 300, Guangzhou Road, Nanjing 210029, Jiangsu Province, P.R. China.
E-mail: lixinhua@njmu.edu.cn

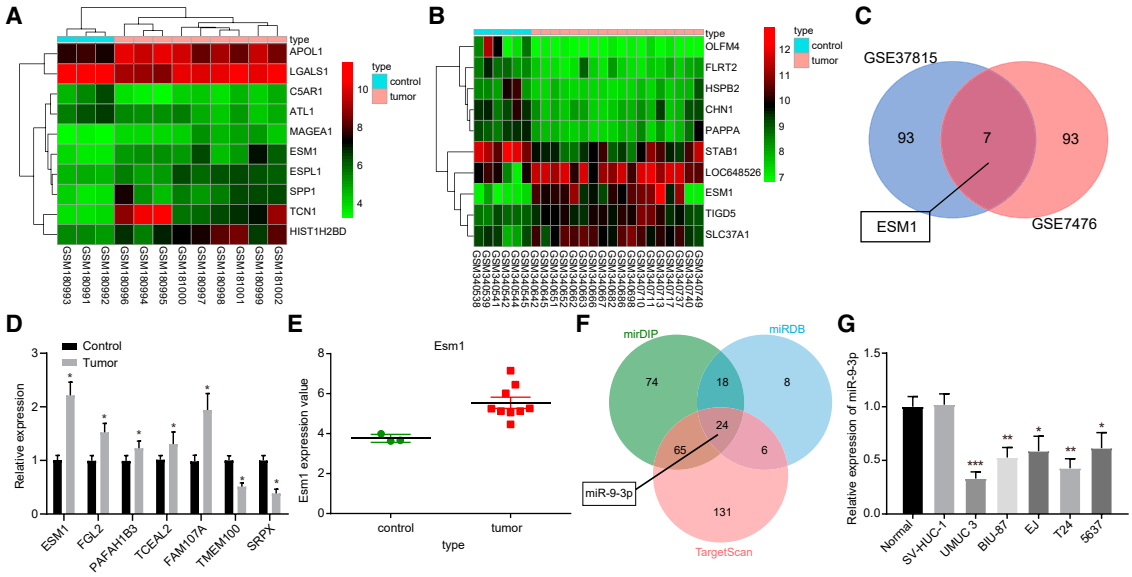

Figure 1. ESM1 Expresses Highly and miR-9-3p Expresses Poorly in Bladder Cancer

(A and B) Heatmaps showing DEGs after analyzing (A) GSE7476 and (B) GSE37815. The x label indicates sample number, and the y label indicates DEGs. Red denotes high expression, whereas green denotes low expression. Each rectangle represents gene expression from one sample. Dendrogram on the left shows gene expression clustering, whereas the upper dendrogram shows sample clustering. (C) Venn diagram showing overlap of DEGs between GSE7476 and GSE37815. (D) qRT-PCR of ESM1 expression in bladder cancer tissues and adjacent normal tissues. (E) Gene expression profiling analysis of ESM1. Green indicates ESM1 gene expression of adjacent normal tissues, and red indicates ESM1 gene expression in bladder cancer tissues. (F) Venn diagram depicting overlap of predicted miRNAs that regulated ESM1. Blue indicates prediction results from miRDB database, red from TargetScan database, and green from mirDIP database. (G) miR-9-3p expression in five bladder cancer cell lines (UMUC-3, BIU-87, EJ, T24, and 5637) and normal bladder epithelial cell line SV-HUC-1 determined by qRT-PCR. *$p < 0.05$ versus adjacent normal tissues; **$p < 0.01$ versus normal primary bladder epithelial cells; ***$p < 0.001$ versus normal bladder epithelial cell line SV-HUC-1. T indicates error bars. Measurement data are presented as mean ± SD. Comparisons among multiple groups are performed using one-way ANOVA. The experiment is repeated three times.

miR-183, miR-96, miR17-5p, and miR-20a are upregulated in this cancer.[10] Other studies have shown that 15 miRNAs are differentially expressed in bladder cancer, such as miR-9, miR-133a, and miR-133b.[11] This study preliminarily explored the potentially modulatory role of miR-9-3p in bladder cancer.

Exosomes from several cell types have been shown to mediate cellular communication and transfer functional miRNAs to regulate target mRNAs.[12] Interestingly, exosomal miR-9-3p suppresses the development and progression of hepatocellular carcinoma.[13] In light of the above results, we determined the relationship between exosomal miR-9-3p and ESM1, and their combined effects on bladder cancer.

RESULTS

Increased ESM1 and Decreased miR-9-3p Expression in Bladder Cancer

Analysis of bladder cancer-related gene expression datasets GSE7476 and GSE37815 obtained seven overlapped genes including ESM1, FGL2, PAFAH1B3, TCEAL2, FAM107A, TMEM100, and SRPX. Next, qRT-PCR was performed to determine their expression levels in bladder cancer tissues and adjacent normal tissues. It was observed that ESM1 expression was increased in bladder cancer tissues ($p < 0.05$) (Figures 1A–1E). Then miRDB, TargetScan, and mirDIP databases predicted that there were 24 miRNAs that might regulate ESM1 expression (Table S1). Among them, miR-9-3p could exert its regulatory function by being encapsulated by exosomes.[13,14] These results suggested that miR-9-3p might regulate the expression of ESM1 (Figure 1F). In addition, qRT-PCR also found that miR-9-3p was differentially expressed in five bladder cancer cell lines (UMUC-3, BIU-87, EJ, T24, and 5637) (Figure 1G). The UMUC-3 cell line had the lowest expression of miR-9-3p ($p < 0.05$). Therefore, the UMUC-3 cell line was selected for subsequent experiments.

BMSCs Inhibit Viability, Migration, and Invasion, and Promote Apoptosis in Bladder Cancer Cells

Mouse bone marrow-derived mesenchymal stem cells (BMSCs) were cocultured with bladder cancer cell line UMUC-3 in a Transwell chamber to determine the effects of BMSCs on bladder cancer cell viability, apoptosis, migration, and invasion (Figures 2A–2D). It was found that compared with the single culture of UMUC-3, their coculture decreased cell viability, invasion, and migration, and increased apoptosis in UMUC-3 cells ($p < 0.05$). Meanwhile, the same experiment was conducted between human BMSCs and bladder cancer cell line UMUC-3, with similar results obtained (Figure S1). These results suggested that BMSCs may have inhibitory effects on bladder cancer cells.

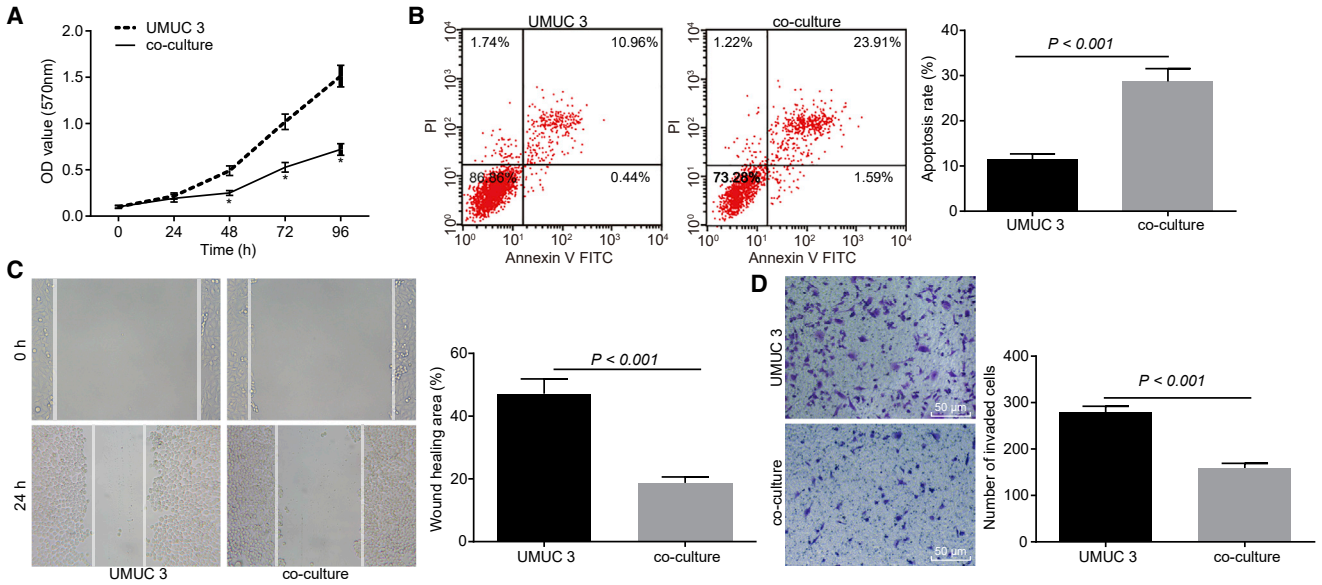

Figure 2. BMSCs Affect the Biological Functions of Bladder Cancer Cell Line UMUC-3

BMSCs of mouse are cocultured with bladder cancer cell line UMUC-3. (A) Cell viability of UMUC-3 measured by MTT assay. (B) Cell apoptosis of UMUC-3 detected by flow cytometry. (C) Cell migration of UMUC-3 determined by scratch test. (D) Cell invasion of UMUC-3 detected by Transwell assay (scale bar = 50 μm). *p < 0.05 versus the culture of UMUC-3 cells alone T indicates error bars.. Measurement data are presented as mean ± SD. Independent sample t test is used for statistical analysis between the two groups. Viability of cells at different time points is analyzed by repeated-measurement ANOVA. The experiment is repeated three times.

Exosome Secreted from BMSCs Affects Biological Functions of Bladder Cancer Cells

The secretion from BMSCs was observed using a transmission electron microscope (HT7700; Beijing SJC Science and Trade, Beijing, China). BMSC secretions had typical exosome morphologies, characterized by irregular sizes and approximate diameter of 30–100 nm (Figure 3A). These secretions had a spherical structure surrounded by a lipid bilayer membrane, which was stained dark outside and lightly stained inside with protein-like substances. Exosome size was further determined using a nanoparticle tracking analyzer (NTA). It was found that the majority of exosomes had a diameter of approximately 120 nm, ranging from 30 to 150 nm. The most abundant exosome size was around 115 nm in diameter and at 1.7×10^{11} particles/L (Figure 3B). For further verification, the expression of exosomal surface marker proteins was determined by western blot analysis. CD9, CD63, CD81, Alix, and TSG101 were all found in exosomes produced by BMSCs, yet there was no presence of nonspecific protein calnexin (Figure 3C). These results strongly suggested that BMSCs secreted exosomes.

Under a confocal microscope, exosomes labeled with PKH26 were cocultured with UMUC-3 cells. After 30 min of coculture, slight red fluorescence of PKH26-labeled exosomes was observed in UMUC-3 cells, suggesting fewer exosomes were present in UMUC-3 cells. With the extension of coculture time, more and more UMUC-3 cells revealed red fluorescence, demonstrating the increase of PKH26-labeled exosomes taken up by UMUC-3 cells. After 24 h of coculture, this was especially clear (Figure 3D). Hence BMSC-derived exosome could be taken up by bladder cancer cells.

To study the effect of exosomes on biological functions of bladder cancer cells *in vitro*, we added a specific exosome secretion inhibitor, GW4869, to the coculture system to assess the release of exosomes. The same concentration of DMSO was added as control. Bicinchoninic acid (BCA) assay, NTA, and western blot analysis found that when compared with the addition of DMSO, the addition of GW4869 decreased total protein concentration and expression of CD9, CD63, CD81, Alix, and TSG101 ($p < 0.05$) (Figures 3E–3I), suggesting decreased exosome secretion. Meanwhile, the addition of GW4869 also increased cell viability, migration, and invasion in bladder cancer cells cocultured with BMSCs.

Next, to exclude other potential disturbances on cells, we examined the effect of GW4869 on single UMUC-3 cells. The addition of GW4869 did not impact cell viability, migration, and invasion of bladder cancer cells ($p > 0.05$) (Figure S2). These results suggest that exosomes secreted by BMSCs may be responsible for the effects of BMSCs on bladder cancer cells.

Exosomal miR-9-3p Inhibits Viability, Migration, and Invasion while Promoting Apoptosis in Bladder Cancer Cells

miR-9-3p in BMSCs was overexpressed to determine its effects on viability, apoptosis, migration, and invasion of bladder cancer cells. Next, exosomes were isolated and purified. qRT-PCR verified that exosomal miR-9-3p expression was increased following treatment

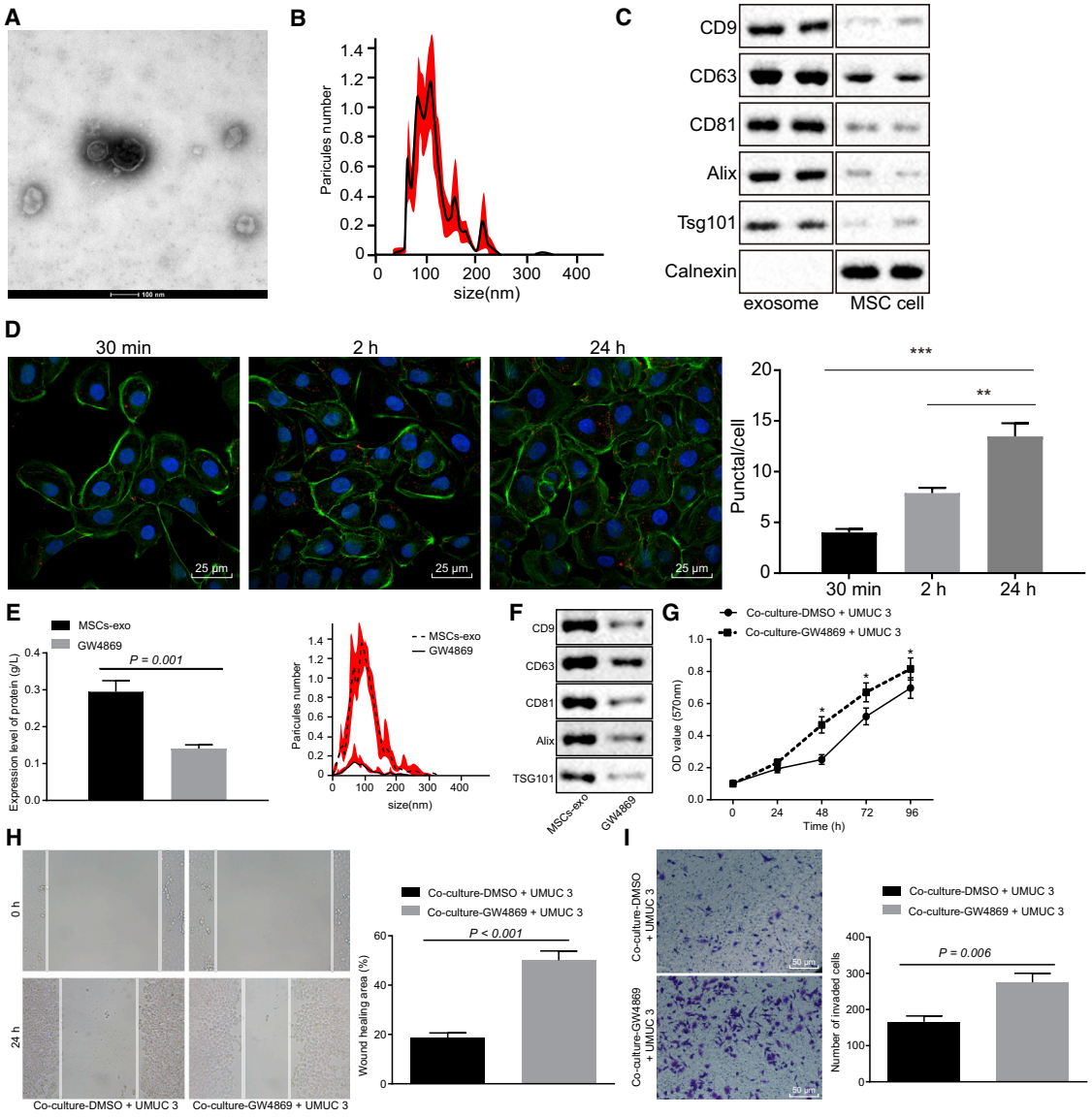

Figure 3. Exosome Secreted from BMSCs Affects Biological Functions of Bladder Cancer Cells

(A) Representative micrographs showing exosome ultrastructure (scale bar = 100 μm). (B) Exosome size and concentration determined by NanoSight particle size analysis. (C) Representative bands showing exosomal surface marker protein expression levels of CD9, CD63, CD81, Alix, TSG101, and Calnexin. (D) Uptake of exosomes by UMUC-3 cells at different time points. Exosomes labeled with PKH26 are stained red, whereas UMUC-3 cells are stained green, and the DAPI nuclei are stained blue. A specific exosome secretion inhibitor GW4869 is added into the coculture system of BMSCs and UMUC-3 cells (scale bar = 25 μm). (E) Exosomal protein expression and concentration determined by BCA assay and NTA. (F) Western blot analysis of exosomal surface marker proteins CD9, CD63, CD81, Alix, TSG101, and Calnexin. (G) UMUC-3 cell viability measured by MTT assay. (H) UMUC-3 cell migration determined by scratch test. (I) UMUC-3 cell invasion examined by Transwell assay (scale bar = 50 μm). Measurement data are presented as mean ± SD. Independent sample t test was used for statistical analysis between the two groups. Viability of cells at different time points is analyzed by repeated-measurement ANOVA. The experiment is repeated three times. *$p < 0.05$ versus the addition of DMSO into the coculture system of BMSCs and UMUC-3 cells; T indicates error bars. **$p < 0.01$ versus Normal-Exo; ***$p < 0.001$ versus the coculture of PKH26-labeled exosomes at different time points.

with Exo-miR-9-3p (BMSC-derived exosomes treated with miR-9-3p mimic) ($p < 0.05$) (Figure 4A). A series of *in vitro* experiments including 3-(4,5-dimethylthiazol-2-yl)-2,5-diphenyltetrazolium bromide (MTT) assay, flow cytometry, scratch test, and Transwell assay were conducted to assess viability, apoptosis, migration, and invasion in bladder cancer cells (Figures 4B–4E). It was revealed that cell viability, migration, and invasion were decreased, whereas apoptosis was increased following the treatment of Exo-miR-9-3p ($p < 0.05$). Additionally, western blot analysis detected that protein expression levels of proliferation-associated factors (Ki67 and

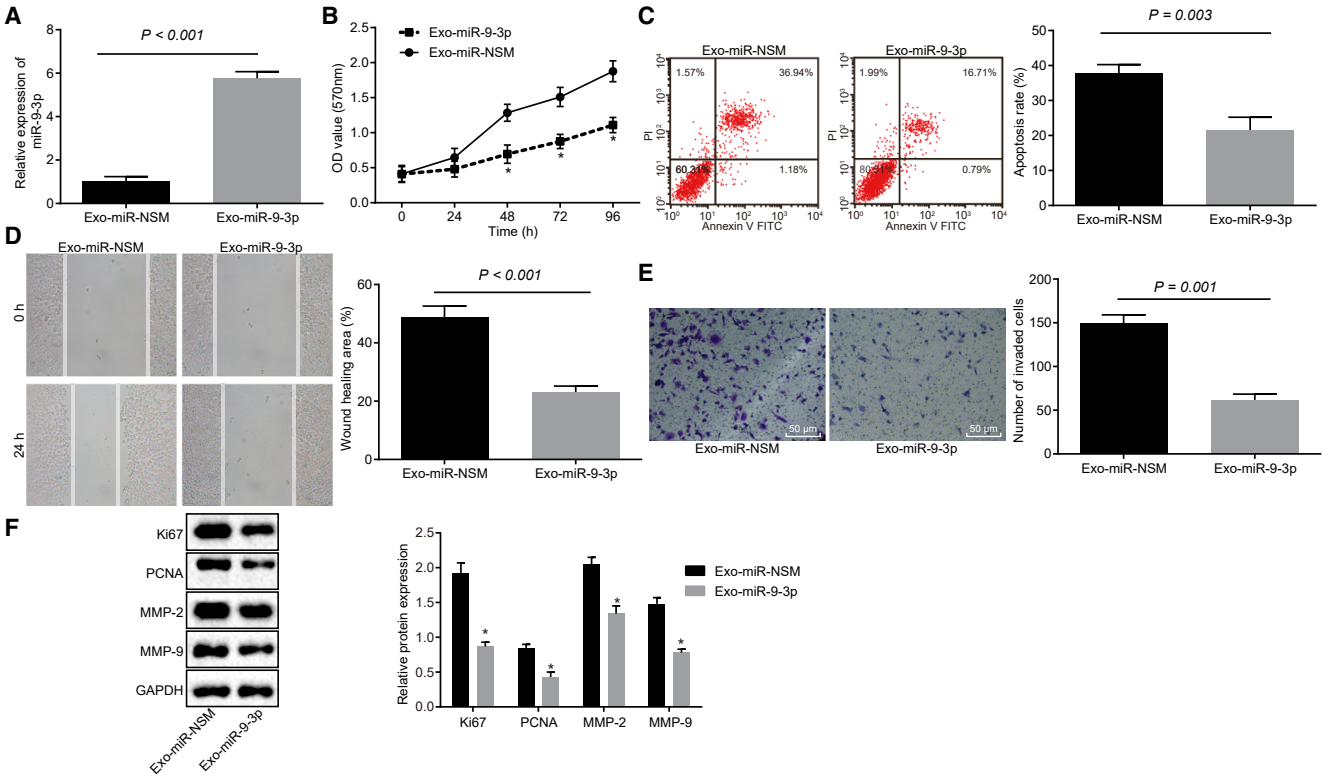

Figure 4. miR-9-3p in Exosomes Suppresses the Viability, Migration, and Invasion of Bladder Cancer Cells, while Promoting Apoptosis

(A) miR-9-3p expression in exosomes. (B) Cell viability by MTT assay. (C) Cell apoptosis by flow cytometry. (D) Cell migration by scratch test. (E) Cell invasion by Transwell assay (scale bar = 50 μm). (F) Protein expression of proliferation-associated factors (Ki67 and PCNA) and invasion-associated factors (MMP-2 and MMP-9) by western blot analysis. T indicates error bars.*p < 0.05 versus the treatment of Exo-miR-NSM (BMSC-derived exosomes treated with miR-mimic control). Measurement data are presented as mean ± SD. Independent sample t test is used for statistical analysis between the two groups. Viability of cells at different time points is analyzed by repeated-measurement ANOVA. The experiment is repeated three times.

proliferating cell nuclear antigen [PCNA]) and invasion-associated factors (matrix metalloprotease [MMP]-2 and MMP-9) were decreased following the treatment of Exo-miR-9-3p ($p < 0.05$) (Figure 4F). Therefore, exosomal miR-9-3p inhibited viability, migration, and invasion, and promoted apoptosis in bladder cancer cells.

miR-9-3p Elevation Impairs Viability, Migration, Invasion, and Apoptosis of Bladder Cancer Cells

In order to investigate the effect of miR-9-3p on the biological functions of bladder cancer cells, miR-9-3p was overexpressed and decreased in bladder cancer cell line UMUC-3 to detect the proliferation, migration, invasion, and apoptosis of bladder cancer cells. It was observed that, when compared with matched controls, the UMUC-3 cell viability, migration, and invasion were decreased and apoptosis was increased in the treatment of mimic miR-9-3p, whereas opposite results were observed in the treatment of inhibitor miR-9-3p ($p < 0.05$) (Figures 5A–5H). All of the results indicated that upregulation of miR-9-3p could inhibit the viability, migration, and invasion, and promote the apoptosis of bladder cancer cells.

miR-9-3p Targets ESM1, and ESM1 Silencing Prevents Bladder Cancer Progression

Previous microarray analysis indicated that ESM1 might be a target gene of miR-9-3p. In the current study, a binding site was identified between miR-9-3p and ESM1 using TargetScan (Figure S3A), which was then verified by dual-luciferase reporter gene assay (Figure S3B). It was found that in the presence of miR-9-3p overexpression (miR-OE) (cells treated with mimic miR-9-3p), the luciferase activity of ESM1-5′ UTR (hsa_miR-9-3p) (wild-type [WT]) showed a decline, whereas that of ESM1-5′ UTR (hsa_miR-9-3p) (mutant [MUT]) did not alter. These results further demonstrated that ESM1 was a target gene of miR-9-3p.

qRT-PCR was used to detect the expression of ESM1 in bladder cancer cells. The results showed that the expression of ESM1 in bladder cancer cells was upregulated ($p < 0.05$) (Figure 6A). ESM1 was decreased to determine its effects on bladder cancer cell viability, migration, invasion, and apoptosis (Figures 6B–6E). It was revealed that cell viability, migration, and invasion were retarded, whereas apoptosis was enhanced after silencing of ESM1.

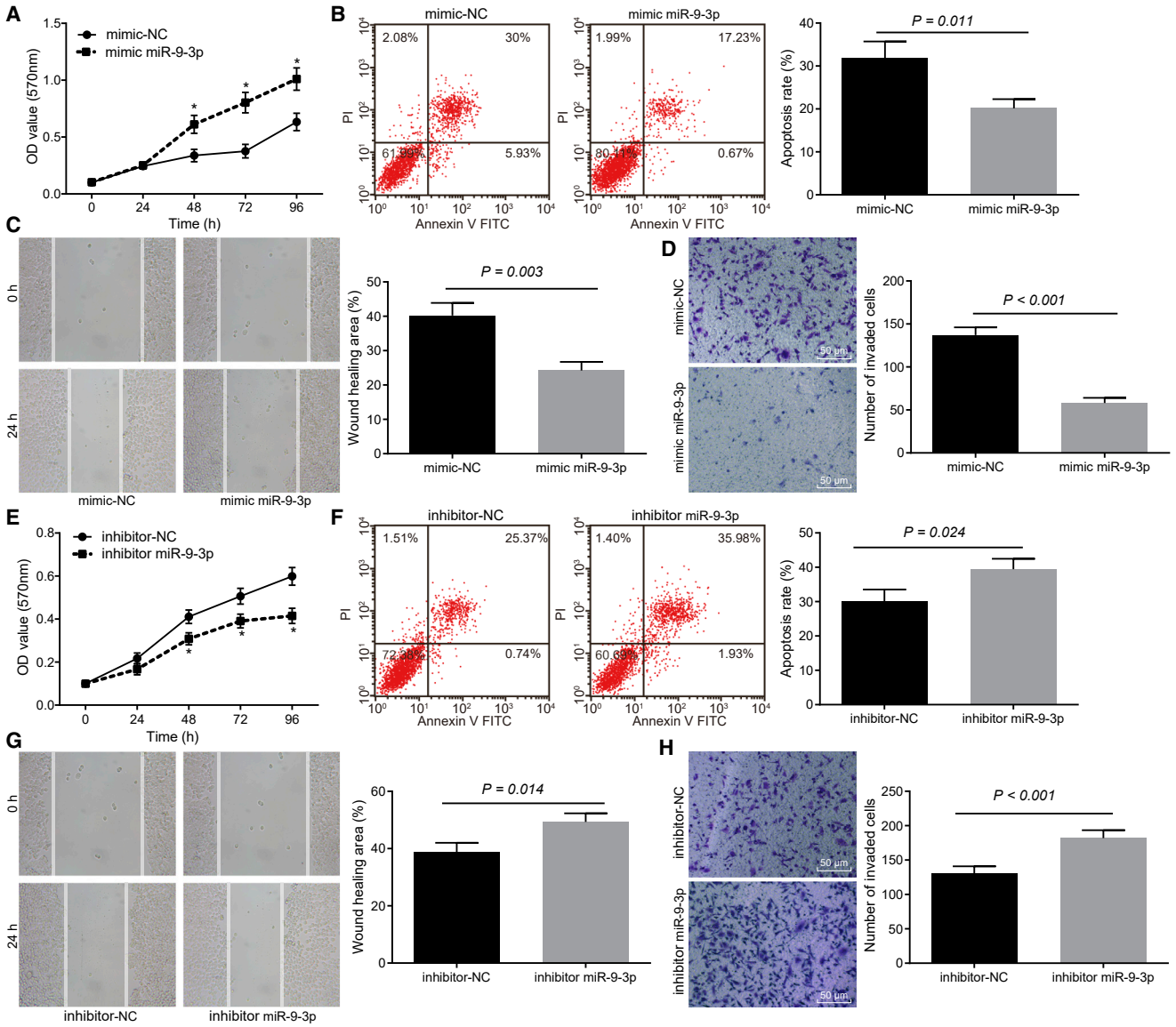

Figure 5. Overexpression of miR-9-3p Represses the Viability, Migration, and Invasion, and Promotes the Apoptosis of Bladder Cancer Cells

(A–D) Effects of miR-9-3p elevation on (A) cell viability, (B) apoptosis, (C) migration, and (D) invasion in bladder cancer cell line UMUC-3 (scale bar = 50 μm). (E–H) Effects of miR-9-3p inhibition on (E) cell viability, (F) apoptosis, (G) migration, and (H) invasion in bladder cancer cell line UMUC-3 (scale bar = 50 μm). T indicates error bars.*p < 0.05 versus the treatment of mimic NC or inhibitor NC. Measurement data are presented as mean ± SD. Independent sample t test is used for statistical analysis between the two groups. Viability of cells at different time points is analyzed by repeated-measurement ANOVA. The experiment is repeated three times.

Next, tumor formation in nude mice was conducted to evaluate the effect of si-ESM1 on tumor growth. It was found that ESM1 expression was decreased after ESM1 was knocked down, and its silencing weakened tumor growth, tumor volume, and tumor weight ($p < 0.05$) (Figures 6F–6I). Concurrently, immunofluorescent staining found that silencing of ESM1 reduced the expression of MMP-2 and MMP-9 ($p < 0.05$) (Figure 6J). H&E staining was then used to examine tumor metastasis to liver. Different degrees of lesions could be observed in nude mice, with silencing of ESM1 yielding improved lesions in liver and a lower number of lymph nodes ($p < 0.05$) (Figure 6K). Moreover, as immunohistochemistry and western blot assays demonstrated, silencing of ESM1 significantly downregulated the expression of ESM1 (Figures 6L and 6M). Therefore, silencing of ESM1 could inhibit bladder cancer distant metastasis and tumor formation in liver.

ESM1 and miR-9-3p were then decreased in bladder cancer cells to test this hypothesis (Figures S4A–S4F). There was no significant difference in the expression of ESM1, cell viability, apoptosis, migration, and invasion following the treatment of inhibitor miR-9-3p + si-ESM1

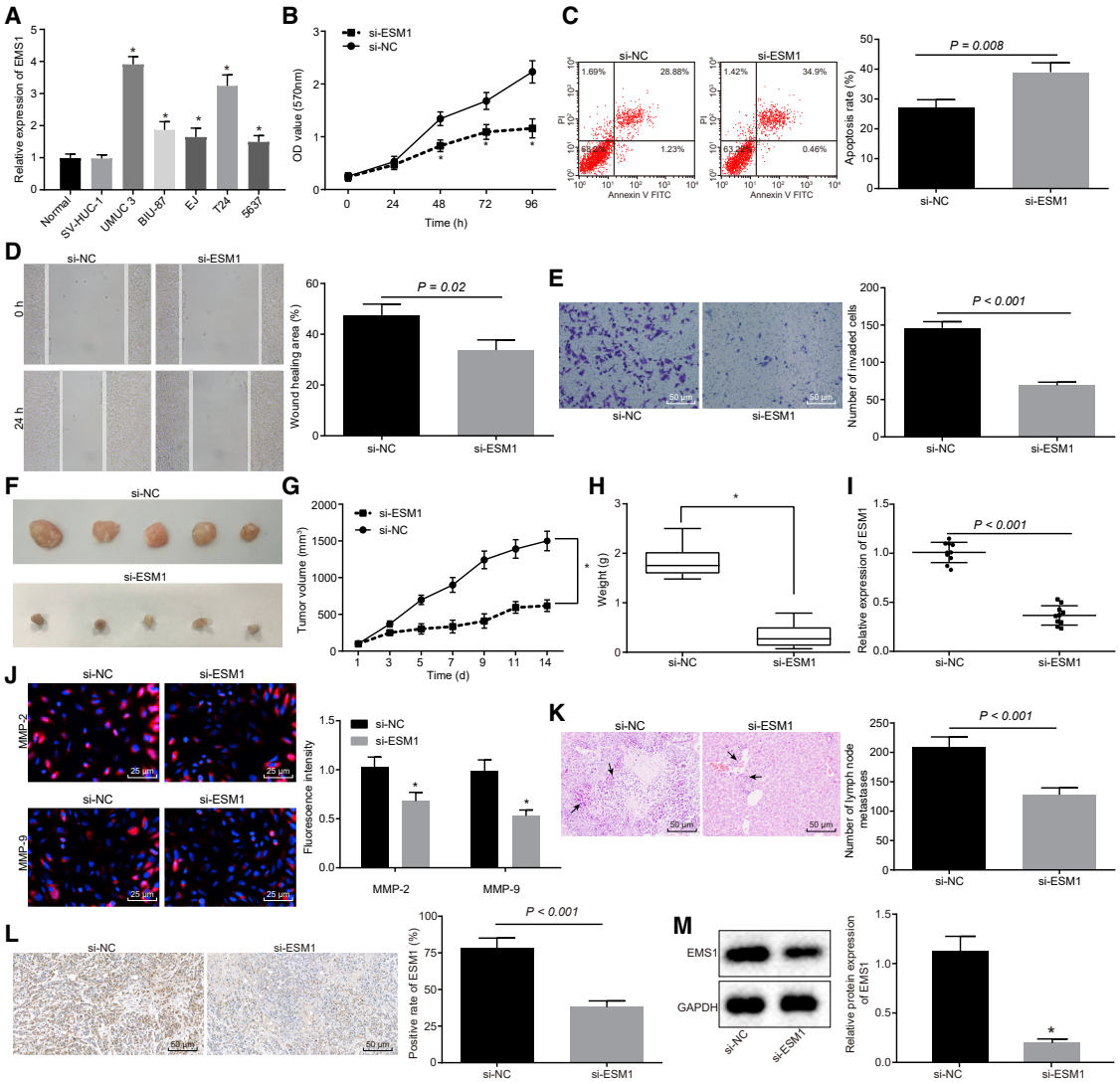

Figure 6. Silencing of ESM1 Disrupts Bladder Cancer Progression

(A) qRT-PCR of ESM1 expression in bladder cancer cells. Bladder cancer cells are treated with si-ESM1 plasmid. (B) Cell viability by MTT assay. (C) Cell apoptosis by flow cytometry. (D) Cell migration by scratch test. (E) Cell invasion by Transwell assay (scale bar = 50 μm). (F) Tumor formed after si-ESM1 treatment in nude mice. (G) Tumor volume after si-ESM1 treatment in nude mice (scale bar = 25 μm). (H) Tumor weight after si-ESM1 treatment in nude mice. (I) ESM1 expression in tumor tissues after si-ESM1 treatment in nude mice detected by qRT-PCR. (J) Immunofluorescence assay to detect the expression of invasion-related factors (MMP-2, MMP-9) in tumor tissues after si-ESM1 treatment in nude mice. (K) Liver tissue slices of nude mice and number of lymph node metastasis by H&E staining after 8 weeks of injection of bladder cancer cells UMUC-3(scale bar = 50 μm). (L) Immunohistochemistry to detect ESM1 expression in tumor tissues after si-ESM1 treatment in nude mice(scale bar = 50 μm). (M) Western blot analysis to detect ESM1 expression in tumor tissues after si-ESM1 treatment in nude mice. T indicates error bars. *p < 0.05 versus the treatment of si-NC. Measurement data are presented as mean ± SD. Independent sample t test is used for statistical analysis between the two groups. Viability of cells at different time points is analyzed by repeated-measurement ANOVA. The experiment is repeated three times. n = 10.

($p > 0.05$). Therefore, silencing ESM1 could repress viability, apoptosis, migration, and invasion of bladder cancer cells.

Exosomal miR-9-3p Upregulation Inhibits Tumor Growth and Metastasis *In Vivo*

Xenograft tumor was used to determine the effect of exosomal miR-9-3p on tumor growth in nude mice. As shown in Figures 7A–7D, miR-9-3p expression was increased after the treatment of Exo-miR-9-3p ($p < 0.05$), whereas exosomal miR-9-3p upregulation decreased tumor growth, tumor volume, and tumor weight ($p < 0.05$). Moreover, the results of immunofluorescent staining demonstrated that exosomal miR-9-3p upregulation decreased MMP-2 and MMP-9 expression ($p < 0.05$) (Figure 7E). In addition, H&E staining was utilized to determined cancer metastasis to liver and lymph node metastasis.

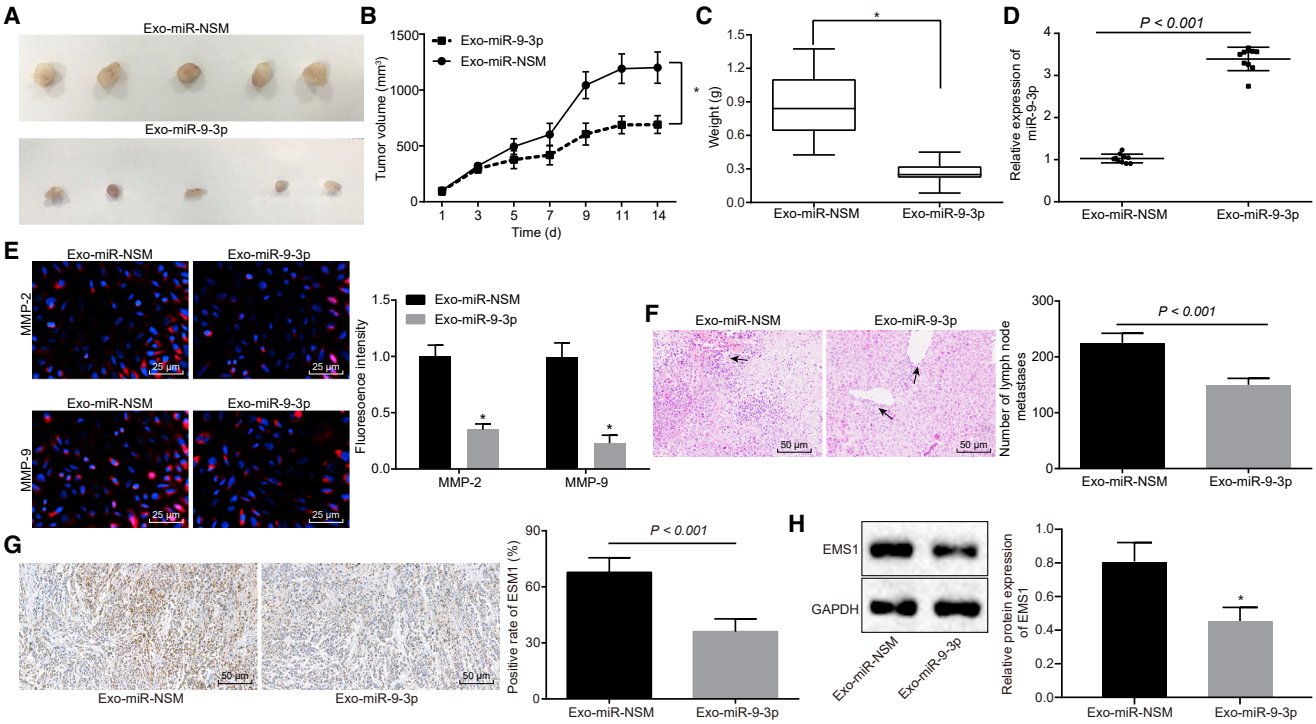

Figure 7. Overexpression of Exosomal miR-9-3p Suppresses the Distant Metastasis of Bladder Cancer Cells and Inhibits the Formation of Liver Tumors

(A) Tumor formed after Exo-miR-9-3p treatment. (B) Tumor volume after Exo-miR-9-3p treatment. (C) Tumor weight after Exo-miR-9-3p treatment. (D) miR-9-3p expression in tumor tissues after Exo-miR-9-3p treatment detected by qRT-PCR. (E) Immunofluorescence assay to detect the expression of invasion-related factors (MMP-2, MMP-9) in tumor tissues after Exo-miR-9-3p treatment (scale bar = 25 μm). (F) Liver tissues of nude mice and number of lymph node metastasis by H&E staining after 3 weeks of injection of bladder cancer cells UMUC-3(scale bar = 50 μm). (G) Immunohistochemistry to detect ESM1 expression in tumor tissues after Exo-miR-9-3p treatment in nude mice (scale bar = 50 μm). (H) Western blot analysis to detect ESM1 expression in tumor tissues after Exo-miR-9-3p treatment in nude mice. T indicates error bars. *p < 0.05 versus the treatment of Exo-miR-NSM. Measurement data are presented as mean ± SD. Independent sample t test is used for statistical analysis between the two groups. Tumor volume at different time points is analyzed by repeated-measurement ANOVA. n = 10.

It was found that exosomal miR-9-3p elevation reduced lesions in the liver and number of lymph node metastasis ($p < 0.05$) (Figure 7F). Additionally, immunohistochemistry and western blot analysis were conducted to determine ESM1 protein expression (Figures 7G and 7H). The results revealed that exosomal miR-9-3p elevation led to a reduction in ESM1 protein expression ($p < 0.05$). Meanwhile, opposite results were detected in the nude mice treated with exosomal miR-9-3p inhibitor, which further verified the above findings (Figures S5A–S5F). Taken together, Exo-miR-9-3p upregulation inhibited tumor growth and metastasis in nude mice.

DISCUSSION

Genome-wide expression and sequencing analyses identify genes and pathways that are responsible for bladder cancer progression and understanding disease heterogeneity and molecular mechanisms.[15] Based on the data from two microarray gene expression profiles, GSE7476 and GSE37815, we identified that ESM1 was elevated in bladder cancer when compared with adjacent normal tissues. Exosomes have been recently recognized to regulate cell functions by transferring miRNAs.[16] Our data agreed with this concept that miR-9-3p upregulation in BMSC-derived exosomes inhibited cellular progression and tumor growth in bladder cancer by targeting ESM1.

One of the important findings in the current study was that miR-9-3p elevation inhibited bladder cancer cell viability, migration, and invasion, and promoted its apoptosis. miRNAs are dysregulated in several urological cancers such as bladder, prostate, and renal cell cancer, and function as regulators of signal transduction.[17] Aberrant miR-9-3p expression has been observed in various types of malignant cancers, thus playing distinct roles in cancer progression. For example, miR-9-3p is proposed as a tumor promoter in medullary thyroid carcinoma cells.[18] In contrast, miR-9-3p acts as a tumor suppressor in other types of cancers. For instance, miR-9-3p reverses the EMT process and restrains proliferation and metastasis in nasopharyngeal carcinoma cells.[19] A transcriptome profile study reveals miR-9-3p as an anti-tumor miRNA that inhibits the invasion of gastric cancer cells. Additionally, miR-9-3p also augments H_2O_2-induced glioma cell apoptosis.[20,21] These previous findings are consistent with our results that miR-9-3p elevation impaired bladder cancer cell viability, migration, and invasion, and enhanced its apoptosis.

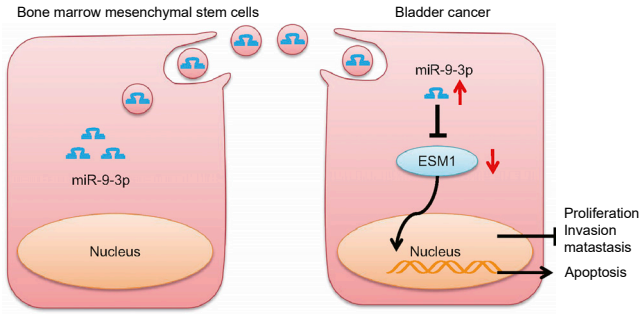

Figure 8. Schematic Diagram Showing Proposed Mechanisms by which Exosomal miR-9-3p Derived from BMSCs Inhibits the Development of Bladder Cancer

Decreased miR-9-3p expression in bladder cancer reduces the inhibitory effect on ESM1. Increased ESM1 expression promotes bladder cancer cell proliferation, invasion, and metastasis, and inhibits apoptosis. miR-9-3p-containing exosomes secreted by BMSCs decrease the expression of ESM1, and hence inhibit bladder cancer cell proliferation, invasion, and metastasis, and promote apoptosis.

Another important finding of this study was that ESM1 was a target gene of miR-9-3p. Similarly, miR-9-3p exhibits a suppressive role in hepatocellular carcinoma by targeting TAZ (WWTR1).[22] Our study also found that ESM1 was expressed at a high level in bladder cancers, and this elevation increased bladder cancer cell viability, migration, and invasion, while inhibiting apoptosis. These findings suggest that ESM1 has an oncogenic property. TCGA bioinformatics database analysis displays that ESM1 is overexpressed in oral squamous cell carcinoma patients when compared with that in normal individuals.[23] Another study also shows that ESM1 exhibits an upregulated expression in prostate tumor tissues.[24] Further, high nuclear expression of ESM1 is detected in metastatic head and neck cancer cells.[25] In addition, a prior study demonstrates that upregulation of ESM1 mRNA level correlates with distant metastasis and vascular invasion in gastric cancer.[26] The same study also unravels that the loss of ESM1 reduces the proliferation and migration activity in head and neck cancer cells.[25] Moreover, ESM1 silencing inhibits colorectal cancer cell migration and invasion,[27] and suppresses hepatocellular carcinoma progression.[28] These findings strongly support our results that ESM1 silencing suppressed bladder cancer cell viability, migration, and invasion, and facilitated its apoptosis.

Our study further identified that miR-9-3p, delivered from BMSC-derived exosomes, exerted anti-tumor effects in both bladder cancer cells and tumor-bearing nude mice. Similarly, exosomal miR-29c has been shown to trigger apoptosis of bladder cancer cells BIU-87 through negative regulation of Bcl-2 and MCL-1, thus preventing bladder cancer progression.[29] These results are consistent with a tumor-suppressive role of exosomal miR-9-3p in hepatocellular carcinoma.[13] This study further provided evidence that MSC-derived exosomes carrying miR-9-3p repressed liver and lymph node metastasis in mouse models. Furthermore, we also found that miR-9-3p reduced the expression of MMP-2 and MMP-9. MMP-2 and MMP-9 are known as markers of cell invasion. Similar to our results, miR-34a inhibits cell migration and invasion through downregulation of MMP-2 and MMP-9.[30] Additionally, overexpression of MMP-2 and MMP-9 is associated with lymph node metastasis in gastric cancer.[31] Therefore, our results provided evidence that exosomal miR-9-3p might exert anti-tumor effects by regulating MMP-2 and MMP-9, which deserved further investigation.

Taken together, results from this study demonstrated an anti-oncogenic role of miR-9-3p in bladder cancer by inhibiting a tumor promoter gene ESM1. Importantly, we demonstrated that miR-9-3p transferred through BMSC-derived exosomes prevented cancer progression and metastasis, which may provide insight on miRNA-based treatment for bladder cancer (Figure 8). However, the specific mechanism that underpins this process remains unclear, with further work required to consolidate this model.

MATERIALS AND METHODS

Ethical Statement

Written informed consent was obtained from all patients prior to the study. Study protocols were approved by Ethics Committee of The Affiliated Cancer Hospital of Nanjing Medical University & Jiangsu Cancer Hospital & Jiangsu Institute of Cancer Research and based on the ethical principles for medical research involving human subjects of the Declaration of Helsinki. All experimental animal protocols were completed in compliance with the *Guide for the Care and Use of Laboratory Animals*[32] and approved by the Animal Care Committee of The Affiliated Cancer Hospital of Nanjing Medical University & Jiangsu Cancer Hospital & Jiangsu Institute of Cancer Research.

Microarray-Based Gene Expression Profiling

Bladder cancer-related microarray expression datasets were downloaded from GEO database (https://www.ncbi.nlm.nih.gov/geo/). The limma package of R language based on Bioconductor software was used to select differentially expressed genes (DEGs) in bladder cancer and control samples using the empirical Bayesian method. A heatmap of DEGs was also constructed with an annotated package of R language. $p < 0.05$ was considered with statistical significance throughout this study. miRDB (http://www.mirdb.org/), TargetScan (http://www.targetscan.org/vert_72/), and mirDIP (http://ophid.utoronto.ca/mirDIP/) databases were used to predict miRNAs that regulated ESM1. A Venn diagram was utilized to compare the predicted results.

Human Bladder Cell Lines

The bladder cancer tissues and adjacent normal tissues were collected from 30 patients who were hospitalized and confirmed as having bladder cancer in The Affiliated Cancer Hospital of Nanjing Medical University & Jiangsu Cancer Hospital & Jiangsu Institute of Cancer Research. The healthy volunteers were all aged over 18 years and without a medical history of urinary disorders.

Human normal bladder epithelial cell line SV-HUC-1 and bladder cancer cell lines (BIU-87, EJ, T24, 5637, and UMUC-3) were

purchased from American Type Culture Collection (Manassas, VA, USA). BMSCs were purchased from Shanghai Fusheng Biotechnology (Shanghai, China).

Cells were cultured with DMEM supplemented with 10% fetal bovine serum (FBS), 100 U/mL penicillin, and 100 mg/mL streptomycin (GIBCO, Gaithersburg, MD, USA) in a humidified incubator at 37°C with 5% CO_2. Culture medium was replaced every 1–2 days. When cells reached 80%–90% confluence, cells were subcultured. The normal primary bladder epithelial cells were isolated and extracted by tissue block culture method as previously described.[33] qRT-PCR was used to determine miR-9-3p expression.

Collection of BMSCs in Mouse

Primary BMSCs were obtained from bilateral tibia and femur in the hind legs of specific pathogen-free (SPF) grade female BALB/c mice (age 4–6 weeks; weight 20–22 g; Hunan SLAC Laboratory Animal, Changsha, Hunan, China). Blood on the bone marrow cavity was washed repeatedly with DMEM with the aid of a 5-mL syringe. Bone marrow suspension was collected and placed in a 10-mL centrifugation tube, and centrifuged at 1,000 rpm for 5 min. After the supernatant was discarded, cells were resuspended in 3 mL of fresh DMEM medium containing 15% FBS. Cell density was adjusted to 1×10^6 cells/mL for inoculation. Cells were then cultured in a culture bottle in an incubator. Cells at passages 2–3 were used for further experiments.

Cell Culture and Transfection

Bladder cancer cell lines UMUC-3 and T24 at logarithmic growth phase and with high expression of ESM1 were plated into a six-well plate (4×10^5 cells/well). When cell confluence reached 70%–80%, cells were transfected according to the instructions of Lipofectamine 2000 (11668-019; Invitrogen, Carlsbad, CA, USA). Next, 200 μL serum-free Opti-MEM was used to dilute 10 μg plasmids (the final concentration into cells was 50 nM) and 5 μL Lipofectamine 2000, respectively. The above diluents were mixed, allowed to stand for 20 min, and cultured in a six-well plate at 37°C with 5% CO_2 and saturated humidity. After 48 h, cells were further cultured in a renewed DMEM containing 20% FBS for 24–48 h for later use. The sequences and plasmids for UMUC-3 transfection including si- negative control (NC), si-ESM1, mimic-NC, mimic miR-9-3p, inhibitor-NC, and inhibitor miR-9-3p were all purchased from Shanghai GenePharma (Shanghai, China).

Afterward, cells in the logarithmic growth phase were transduced with lentivirus when cell confluence reached 30%. Then 1 mL serum-free medium containing 100 U/mL penicillin/streptomycin was transduced with 2×10^6 transducing units (TU) lentivirus and 8 μg/mL Polybrene (H9268; Sigma-Aldrich Chemical Company, St. Louis, MO, USA), which was observed under an inverted fluorescent microscope after 2–3 days. After 48 h, each well was added with 1 μg/mL puromycin (P8833; Sigma-Aldrich Chemical Company, St. Louis, MO, USA) to screen out stably transduced cells, which were then cultured in conventional medium.

Subsequently, BMSCs were transduced with mimic miR-NSM, mimic miR-9-3p, inhibitor miR-NSM, and inhibitor miR-9-3p. After exosomes were derived from BMSCs, they were transduced with Exo-miR-NSM, Exo-miR-9-3p, inhibitor Exo-miR-NSM, and inhibitor Exo-miR-9-3p. qRT-PCR was conducted to determine the expression of miR-9-3p and ESM1.

Coculture of Bladder Cancer Cells and BMSCs or BMSC-Derived Exosomes

BMSCs were detached and plated in a 24-well plate (9×10^3 cells/well) and in a 6-well plate (4.5×10^4 cells/well) (Millipore, Billerica, MA, USA), which were then cultured in DMEM low-glucose medium (the apical chamber). Meanwhile, bladder cancer cells were detached, plated in a 24-well plate (3×10^3 cells/well) and in a 6-well plate (1.5×10^4 cells/well), and cultured in DMEM (the basolateral chamber). After 24 h of culture, the complete medium was removed, and the plate and chambers were irrigated with serum-free DMEM. Cells were then cocultured in DMEM by placing chambers in the wells of culture plates. After that, the apical chamber was removed, and cells were used in subsequent experiments.

Next, BMSC-derived exosomes were incubated with the supernatant of the bladder cancer cell culture medium plated in a 24-well plate with 50%–60% cell confluence for 24 h. Then cells were treated with Exo-mimic-NSM, Exo-miR-9-3p, inhibitor Exo-NSM, and inhibitor Exo-miR-9-3p. qRT-PCR was performed to detect the expression of miR-9-3p and ESM1.

Fluorescent Labeling and Transfer of Exosomes

The extracted exosomes were labeled with the lipophilic dye PKH26 (red) liquor (MINI26-1KT; Sigma-Aldrich Chemical Company, St. Louis, MO, USA) at a working concentration of 10 μM and incubated at 37°C for 20 min. After rinsed by PBS, labeled exosomes were centrifuged at 4°C and 12,000 × *g* for 70 min. The bladder cancer cells (3×10^4 cells/well) grown on coverslips were incubated with PKH26-labeled exosomes at a concentration of 25 μg/mL in a 24-well format for 24 h. Later, the cytoskeleton of bladder cancer cells was selectively stained with fluorescein isothiocyanate (FITC) phalloidin (Yeasen Company, Shanghai, China), resuspended in 500 μL PBS, and stained with DAPI. At last, the internalization of exosomes was measured using a confocal microscope.

Dual-Luciferase Reporter Gene Assay

To verify whether ESM1 was a direct target gene of miR-9-3p, we introduced synthesized ESM1 3′ UTR gene fragment into pMIR-reporter (Beijing Huayueyang Biotechnology, Beijing, China) using SpeI and Hind III sites. Complementary sequence mutation site of the seed sequence was designed on the ESM1-WT. Target fragment was inserted into pMIR-reporter plasmid using T4 DNA ligase after restriction endonuclease digestion. Luciferase reporter plasmids (ESM1-WT and MUT) with correct sequence were cotransfected with miR-9-3p into HEK293T cells (Shanghai Beinuo Biotechnology, Shanghai, China). After 48 h of transfection, cells were collected and lysed, and the luciferase activity was detected using

Table 1. Primer Sequences for qRT-PCR

Gene	Sequence
miR-9-3p	F: 5′-GGAGACCGGAAATGTAGCCA-3′
	R: 5′-AATGGCCCGTGGAGTCTTTG-3′
U6	F: 5′-CTCGCTTCGGCAGCACA-3′
	R: 5′-AACGCTTCACGAATTTGCGT-3′
ESM1	F: 5′-TCAGCGAGTACTTCCTAAAT-3′
	R: 5′-TCTCCTTC TAGAGCGTTACA-3′
GAPDH	F: 5′-TTCACCACCATGGAGAAGGC-3′
	R: 5′-GGCATGGACTGTGGTCATGA-3′

ESM1, endothelial cell-specific molecule 1; F, forward; GAPDH, glyceraldehyde phosphate dehydrogenase; miR-9-3p, microRNA-9-3p; R, reverse.

a luciferase detection kit (K801-200; Biovision, Mountain View, CA, USA) by a Glomax20/20 luminometer (Promega, Madison, WI, USA).

RNA Isolation and Quantification

Total RNA in cells was extracted using a TRIzol kit (Invitrogen, Carlsbad, CA, USA). RNA concentration was determined by NanoDrop 2000 (Thermo Scientific, Wilmington, DE, USA). RNA (1 μg) was then reverse transcribed into the cDNA following the instructions of PrimeScript RT Reagent Kit by a gDNA Eraser (Takara Bio, Tokyo, Japan). qRT-PCR was performed using a SYBR Premix Ex Taq (Tli RNaseH Plus) reagent kit (Takara Bio, Tokyo, Japan) by an ABI7500 real-time quantitative PCR system (Thermo Scientific, Wilmington, DE, USA). Primer sequences (Shanghai GenePharma, Shanghai, China) are listed in Table 1. β-actin or U6 was used as endogenous controls. Fold changes in expression were calculated by the $2^{-\Delta\Delta Ct}$ method.[34]

Western Blot Analysis

Total proteins were extracted from cells, and their concentrations were determined using a BCA kit (Thermo Scientific, Wilmington, DE, USA). Proteins were then separated by PAGE and transferred onto a polyvinylidene difluoride membrane (Amersham Bioscience, Piscataway, NJ, USA). After blocked with 5% skimmed milk at room temperature for 1 h, the membrane was incubated with rabbit monoclonal antibody against CD9 (1:1,000, ab92726), CD81 (1:1,000, ab109201), CD63 (1:1,000, ab134045), TSG101 (1:1,000, ab125011), Ki67 (1:5,000, ab92742), MMP-2 (1:1,000, ab37150), and rabbit polyclonal antibody against Alix (1:1,000, ab76608), Calnexin (1:1,000, ab22595), PCNA (1:1,000, ab18197), MMP-9 (1:1,000, ab73734), and glyceraldehyde phosphate dehydrogenase (GAPDH; 1:1,000, ab37150) overnight at 4°C. The above antibodies were purchased from Abcam (Cambridge, UK). After washed by PBS containing 0.1% Tween 20 (TBST), the membrane was then further incubated with horseradish peroxidase (HRP)-conjugated secondary goat anti-rabbit antibody against immunoglobulin G (IgG; 1:10,000; Jackson ImmunoResearch, West Grove, PA, USA) for 1 h at room temperature. After protein bands were visualized by an optical luminometer (GE Medical Systems, Milwaukee, WI, USA), relative protein expression in each band was measured by Image-Pro Plus 6.0 (Media Cybernetics, Rockville, MD, USA).

MTT Assay

Cells in the logarithmic growth phase were cultured for 24 h. Next, cells were washed twice in PBS, detached with 0.25% trypsin, and centrifuged at 1,000 rpm for 5 min. The uniform single-cell suspension was prepared by a pipette. Cells were then plated in a 96-well plate at the density of 5×10^3 cells/well and cultured in an incubator at 37°C and with 5% CO_2. Six parallel wells were set for each sample. After culture for 24, 48, 72, and 96 h, each well was incubated with 10 μL MTT solution in a 5% CO_2 incubator at 37°C for 2 h. Optical density (OD) in each well was detected at 450 nm by an automatic microplate reader (Multiskan MK3; Thermo, Waltham, MA, USA). The cell growth curve was plotted with the average OD value as the y label and time as the x label to calculate cell viability.

Scratch Test

After 48 h of transfection, cells were settled on the bottom of a six-well plate (Dow Corning, Midland, MI, USA). Cell surface was scratched with a 10-μL pipette head perpendicular to the plate. After washing with PBS three times, cells were added with serum-free DMEM (Nanjing SenBeiJia Biological Technology, Nanjing, China) for observation under an inverted microscope (XDS-800D; Shanghai Caikon Optical Instrument, Shanghai, China). Cells were then incubated for 24 h, and the healing of the scratch area was determined. Healing rate was calculated in three randomly selected visual fields, as the area at 24 h/the area at 0 h area.

Transwell Assay

After 48 h of transfection, cells were starved in serum-free medium for 24 h, washed twice with PBS, and resuspended in serum-free DMEM (Nanjing Sen BeiJia Biological Technology, Nanjing, China) containing 10 g/L BSA. Cell density was adjusted into 3×10^4 cells/mL. The Transwell chamber was placed into a 24-well plate. The apical membrane on the bottom of the Transwell chamber was covered by Matrigel (Millipore, Billerica, MA, USA). After standard detachment procedures, cells were rinsed twice with PBS and resuspended with DMEM, with cell density adjusted to 1×10^5 cells/mL. Then 200-μL cell suspension was added to the apical chamber of the Transwell chamber, whereas 600 μL DMEM containing 20% FBS was added into the basolateral chamber. After 24 h of incubation, the Transwell chamber was removed and cells on the apical chamber were removed by cotton swabs. Cells were fixed with 4% paraformaldehyde, stained with 0.5% crystal violet solution, and washed three times with PBS for 15 min. Afterward, cells were observed and imaged in five randomly selected fields under an inverted microscope (XDS-800D; Shanghai Caikon Optical Instrument, Shanghai, China). The number of transmembrane cells was counted, and cell migration and invasion rate were calculated.

Flow Cytometry

Annexin V FITC/propidium iodide (PI) double staining was used to detect cell apoptosis. After 48 h of transfection, cell concentration was adjusted to 1×10^6 cells/mL. Cells were fixed by 70% precooled ethanol solution overnight at 4°C, and then 100-μL cell suspensions (no less than 10^6 cells/mL) were resuspended in 200 μL binding buffer. Subsequently, cells were stained with 10 μL Annexin V-FITC and 5 μL PI for 15 min at room temperature in the dark. After the addition of 300 μL binding buffer, cell apoptosis was determined by flow cytometry at the excitation wavelength of 488 nm. The flow cytometer was used to analyze 2×10^4 cells each time.

Exosome Isolation

Exosomes were isolated from BMSCs. BMSCs were cultured in 8 × P150 plate for 72 h. Culture medium was collected and centrifuged at 300 × *g* for 10 min to remove cell debris. After centrifuged at 2,000 × *g* for 10 min to remove dead cells, the supernatant was collected and centrifuged again at 100,000 × *g* for 70 min. The pellets were collected, washed with PBS, and centrifuged at 100,000 × *g* for 70 min. The final pellets were resuspended in PBS. Exosomal protein concentration was determined by BCA protein assay (Thermo Scientific, Wilmington, DE, USA).

Transmission Electron Microscope Observation

Isolated exosomes were immediately fixed in 4% glutaraldehyde at 4°C for 2 h, rinsed three times with 0.1 mol/L PBS, and fixed with 1% osmium tetroxide for another 2 h. Subsequently, the exosomes were dehydrated by conventional ethanol and gradient acetone, impregnated with epoxy resin, embedded, and polymerized. Sections of 0.5-μm thickness were prepared under a light microscope, and then ultra-thin sections of 60-nm thickness were prepared, which were stained with uranium acetate and lead citrate, and observed under a transmission electron microscope (HT7700; Beijing SJC Science and Trade, Beijing, China).

NanoSight Nanoparticle Tracking Analysis

Exosomes (20 μg) were dissolved in 1 mL PBS and stirred for 1 min to keep exosomes in uniform distribution. The size of exosomes was observed by NanoSight NTA (Malvern Instruments, UK).

Uptake of Exosomes by Bladder Cancer Cells

PKH26 dye was diluted 1,000 times and added into 20 μg exosome suspension at 37°C for 15 min. Next, the mixed liquor was washed by PBS once and centrifuged at 100,000 × *g* for 70 min. Then PKH26 labeled-exosomes were cocultured with bladder cancer cells for 0.5, 2, and 24 h. Uptake of exosomes by bladder cancer cells was observed under a confocal fluorescence microscope.

BCA Assay

Purified exosomes (18 μL) were plated in a 96-well plate with 2 μL PBS. Total exosomal protein concentration was measured by BCA protein quantitative reagent kit (Thermo Scientific, Wilmington, DE, USA). Total exosomal protein mass = concentration × volume.

Tumor Xenograft in Nude Mice

The SPF grade female BALB/c nude mice (aged 4–6 weeks; weight 14–22 g; Shanghai Experimental Animal Center of Chinese Academy of Sciences, Shanghai, China) were housed at a constant temperature of 25°C–27°C and humidity of 45%–50%. Following anesthesia, the mice were inoculated with cells. Cells in logarithmic growth phase were resuspended in serum-free DMEM (Nanjing SenBeiJia Biological Technology, Jiangsu, China), with the cell concentration adjusted into 4×10^6 cells/mL. Next, 0.5 mL single-cell suspension containing 2×10^6 cells was subcutaneously injected into the left armpit of nude mice. Nude mice were randomly assigned into six groups (10 mice/group). Five nude mice in each group were used for subcutaneous tumorigenesis, and another five nude mice were used for tumor metastasis *in vivo*. Cell suspension was injected into the center of the liver inner membrane of nude mice. After 7 days, the plasmids of Exo-miR-NSM, Exo-miR-9-3p, inhibitor Exo-miR-NSM, and inhibitor Exo-miR-9-3p (the concentration of exosomes was 50 μg/100 μL) were injected into the nude mice by tail vein injection. Then 1×10^8 plaque-forming units (PFUs)/100 μL lentivirus vectors of si-NC and si-ESM1 were transduced into nude mice by tail injection. On the 3rd, 5th, 7th, 9th, 11th, and 14th days after inoculation, the tumor size was measured by a vernier caliper, and the tumor volume (mm^3) was calculated as $(L \times W^2)/2$, where L denoted tumor length and W denoted tumor width. Nude mice were euthanized on the 20th day, and the tumor was collected and weighed. Liver tissues were collected, sliced, and stained with H&E for observing cell metastasis *in vivo*. At last, the number of metastatic nodules in liver tissues was counted.

Immunohistochemistry

Paraffin-embedded slices were dewaxed, dehydrated by gradient ethanol, rinsed under running water for 2 min, and immersed in 3% methanol H_2O_2 for 20 min. Next, the slices were rinsed with distilled water for 2 min and 0.1 M PBS for 3 min, treated with antigen retrieval on water bath, and cooled down in running water. Then slices were sealed with normal goat serum confining liquid (C-0005; Shanghai Haoran Biological Technology, Shanghai, China) at room temperature for 20 min. Later, the slices were probed with primary antibody specific for ESM1 (ab224591, 1:50) at 4°C overnight and second goat anti-rabbit antibody specific for IgG at 37°C for 20 min. Afterward, the slices were added with HRP-labeled streptomycin protein working solution (0343-10000U; Yi Mo Biological Technology, Beijing, China) at 37°C for 20 min. Following that, the slices were visualized by diaminobenzidine (DAB) (ST033; Whiga Biosmart, Guangzhou, Guangdong, China), counterstained by hematoxylin (PT001; Shanghai Bogoo Biological Technology, Shanghai, China) for 1 min, blued by 1% ammonium hydroxide, dehydrated by gradient ethanol, cleared by xylene, mounted with neutral gum, and observed under a microscope. Five high-power fields were randomly selected from each slice, with 100 cells counted in each field. Based on the staining status, specimens with 50% or more positive cancer cells were judged as strong positive; those whose positive cells counted between 10% and 50% were positive and those with less than 10% cancer cells were negative..

Immunofluorescence Staining

The slices were deparaffinized, hydrated, treated with sodium citrate-citric acid antigen retrieval buffer solution, boiled in a pressure cooker for 10 min, and cooled down to room temperature. Next, the slices were sealed with normal goat serum at room temperature for 15 min and then incubated with fluorescence primary antibody against MMP-2 (1:1,000, ab37150; Abcam, Cambridge, UK) and MMP-9 (1:500, ab38898; Abcam, Cambridge, UK). After that, the slices were incubated with fluorescence secondary antibody (1:500) at room temperature for 2 h in darkness, stained with DAPI (1:100, ab104139; Abcam, Cambridge, UK) at room temperature for 10 min in a dark place, sealed by mounting medium, and observed under an inverted fluorescence microscope.

Statistical Analysis

All experimental data were processed and analyzed using SPSS 21.0 (IBM, Armonk, NY, USA). Data were presented as mean ± SD. Data comparisons between two groups were performed by independent sample t test with Welch correction. Shapiro-Wilk test was used to analyze data normality. One-way ANOVA was used to compare data that were normally distributed among multiple groups. Otherwise, the non-parametric Kruskal-Wallis test was used. Cell viability and tumor volume at different time points were analyzed by repeated-measures ANOVA. Differences were considered statistically significant when $p < 0.05$.

SUPPLEMENTAL INFORMATION

Supplemental Information can be found online at https://doi.org/10.1016/j.omtn.2019.09.023.

AUTHOR CONTRIBUTIONS

H.C., X.Y., and Y.G. designed the study. Z.X., B.Y., and T.X. collated the data, carried out data analyses, and produced the initial draft of the manuscript. W.X. revised the figures and tables. X.L., X.W., and L.H. contributed to drafting the manuscript. All authors have read and approved the final submitted manuscript.

CONFLICTS OF INTEREST

The authors declare no competing interests.

ACKNOWLEDGMENTS

We acknowledge and appreciate our colleagues for their valuable efforts and comments on this paper. This study was supported by Research Projects for Health Care for Cadres in Jiangsu Province (grant BJ17031).

REFERENCES

1. Czerniak, B., Dinney, C., and McConkey, D. (2016). Origins of Bladder Cancer. Annu. Rev. Pathol. *11*, 149–174.
2. Siegel, R.L., Miller, K.D., and Jemal, A. (2019). Cancer statistics, 2019. CA Cancer J. Clin. *69*, 7–34.
3. Kamat, A.M., Hahn, N.M., Efstathiou, J.A., Lerner, S.P., Malmström, P.U., Choi, W., Guo, C.C., Lotan, Y., and Kassouf, W. (2016). Bladder cancer. Lancet *388*, 2796–2810.
4. Choi, W., Ochoa, A., McConkey, D.J., Aine, M., Höglund, M., Kim, W.Y., Real, F.X., Kiltie, A.E., Milsom, I., Dyrskjøt, L., and Lerner, S.P. (2017). Genetic Alterations in the Molecular Subtypes of Bladder Cancer: Illustration in the Cancer Genome Atlas Dataset. Eur. Urol. *72*, 354–365.
5. Robertson, A.G., Kim, J., Al-Ahmadie, H., Bellmunt, J., Guo, G., Cherniack, A.D., Hinoue, T., Laird, P.W., Hoadley, K.A., Akbani, R., et al. (2017). Comprehensive molecular characterization of muscle-invasive bladder cancer. Cell *171*, 540–556.e25.
6. Rocha, S.F., Schiller, M., Jing, D., Li, H., Butz, S., Vestweber, D., Biljes, D., Drexler, H.C., Nieminen-Kelhä, M., Vajkoczy, P., et al. (2014). Esm1 modulates endothelial tip cell behavior and vascular permeability by enhancing VEGF bioavailability. Circ. Res. *115*, 581–590.
7. Roudnicky, F., Poyet, C., Wild, P., Krampitz, S., Negrini, F., Huggenberger, R., Rogler, A., Stöhr, R., Hartmann, A., Provenzano, M., et al. (2013). Endocan is upregulated on tumor vessels in invasive bladder cancer where it mediates VEGF-A-induced angiogenesis. Cancer Res. *73*, 1097–1106.
8. Laloglu, E., Aksoy, H., Aksoy, Y., Ozkaya, F., and Akcay, F. (2016). The determination of serum and urinary endocan concentrations in patients with bladder cancer. Ann. Clin. Biochem. *53*, 647–653.
9. Di Leva, G., Garofalo, M., and Croce, C.M. (2014). MicroRNAs in cancer. Annu. Rev. Pathol. *9*, 287–314.
10. Yoshino, H., Seki, N., Itesako, T., Chiyomaru, T., Nakagawa, M., and Enokida, H. (2013). Aberrant expression of microRNAs in bladder cancer. Nat. Rev. Urol. *10*, 396–404.
11. Pignot, G., Cizeron-Clairac, G., Vacher, S., Susini, A., Tozlu, S., Vieillefond, A., Zerbib, M., Lidereau, R., Debre, B., Amsellem-Ouazana, D., and Bieche, I. (2013). microRNA expression profile in a large series of bladder tumors: identification of a 3-miRNA signature associated with aggressiveness of muscle-invasive bladder cancer. Int. J. Cancer *132*, 2479–2491.
12. Stoorvogel, W. (2012). Functional transfer of microRNA by exosomes. Blood *119*, 646–648.
13. Tang, J., Li, Y., Liu, K., Zhu, Q., Yang, W.H., Xiong, L.K., and Guo, D.L. (2018). Exosomal miR-9-3p suppresses HBGF-5 expression and is a functional biomarker in hepatocellular carcinoma. Minerva Med. *109*, 15–23.
14. Joerger-Messerli, M.S., Oppliger, B., Spinelli, M., Thomi, G., di Salvo, I., Schneider, P., and Schoeberlein, A. (2018). Extracellular Vesicles Derived from Wharton's Jelly Mesenchymal Stem Cells Prevent and Resolve Programmed Cell Death Mediated by Perinatal Hypoxia-Ischemia in Neuronal Cells. Cell Transplant. *27*, 168–180.
15. Knowles, M.A., and Hurst, C.D. (2015). Molecular biology of bladder cancer: new insights into pathogenesis and clinical diversity. Nat. Rev. Cancer *15*, 25–41.
16. Melo, S.A., Sugimoto, H., O'Connell, J.T., Kato, N., Villanueva, A., Vidal, A., Qiu, L., Vitkin, E., Perelman, L.T., Melo, C.A., et al. (2014). Cancer exosomes perform cell-independent microRNA biogenesis and promote tumorigenesis. Cancer Cell *26*, 707–721.
17. Fendler, A., Stephan, C., Yousef, G.M., and Jung, K. (2011). MicroRNAs as regulators of signal transduction in urological tumors. Clin. Chem. *57*, 954–968.
18. Chen, Y., Zhang, S., Zhao, R., Zhao, Q., and Zhang, T. (2017). Upregulated miR-9-3p Promotes Cell Growth and Inhibits Apoptosis in Medullary Thyroid Carcinoma by Targeting BLCAP. Oncol. Res. *25*, 1215–1222.
19. Ding, Y., Pan, Y., Liu, S., Jiang, F., and Jiao, J. (2017). Elevation of MiR-9-3p suppresses the epithelial-mesenchymal transition of nasopharyngeal carcinoma cells via down-regulating FN1, ITGB1 and ITGAV. Cancer Biol. Ther. *18*, 414–424.
20. Meng, Q., Xiang, L., Fu, J., Chu, X., Wang, C., and Yan, B. (2017). Transcriptome profiling reveals miR-9-3p as a novel tumor suppressor in gastric cancer. Oncotarget *8*, 37321–37331.
21. Yang, L., Mu, Y., Cui, H., Liang, Y., and Su, X. (2017). MiR-9-3p augments apoptosis induced by H2O2 through down regulation of Herpud1 in glioma. PLoS ONE *12*, e0174839.
22. Higashi, T., Hayashi, H., Ishimoto, T., Takeyama, H., Kaida, T., Arima, K., Taki, K., Sakamoto, K., Kuroki, H., Okabe, H., et al. (2015). miR-9-3p plays a tumour-suppressor role by targeting TAZ (WWTR1) in hepatocellular carcinoma cells. Br. J. Cancer *113*, 252–258.

23. Yang, W.E., Hsieh, M.J., Lin, C.W., Kuo, C.Y., Yang, S.F., Chuang, C.Y., and Chen, M.K. (2017). Plasma Levels of Endothelial Cell-Specific Molecule-1 as a Potential Biomarker of Oral Cancer Progression. Int. J. Med. Sci. *14*, 1094–1100.

24. Lai, C.Y., Chen, C.M., Hsu, W.H., Hsieh, Y.H., and Liu, C.J. (2017). Overexpression of Endothelial Cell-Specific Molecule 1 Correlates with Gleason Score and Expression of Androgen Receptor in Prostate Carcinoma. Int. J. Med. Sci. *14*, 1263–1267.

25. Bender, O., Gunduz, M., Cigdem, S., Hatipoglu, O.F., Acar, M., Kaya, M., Grenman, R., Gunduz, E., and Ugur, K.S. (2018). Functional analysis of ESM1 by siRNA knockdown in primary and metastatic head and neck cancer cells. J. Oral Pathol. Med. *47*, 40–47.

26. Liu, N., Zhang, L.H., Du, H., Hu, Y., Zhang, G.G., Wang, X.H., Li, J.Y., and Ji, J.F. (2010). Overexpression of endothelial cell specific molecule-1 (ESM-1) in gastric cancer. Ann. Surg. Oncol. *17*, 2628–2639.

27. Kang, Y.H., Ji, N.Y., Han, S.R., Lee, C.I., Kim, J.W., Yeom, Y.I., Kim, Y.H., Chun, H.K., Kim, J.W., Chung, J.W., et al. (2012). ESM-1 regulates cell growth and metastatic process through activation of NF-κB in colorectal cancer. Cell. Signal. *24*, 1940–1949.

28. Kang, Y.H., Ji, N.Y., Lee, C.I., Lee, H.G., Kim, J.W., Yeom, Y.I., Kim, D.G., Yoon, S.K., Kim, J.W., Park, P.J., and Song, E.Y. (2011). ESM-1 silencing decreased cell survival, migration, and invasion and modulated cell cycle progression in hepatocellular carcinoma. Amino Acids *40*, 1003–1013.

29. Xu, X.D., Wu, X.H., Fan, Y.R., Tan, B., Quan, Z., and Luo, C.L. (2014). Exosome-derived microRNA-29c induces apoptosis of BIU-87 cells by down regulating BCL-2 and MCL-1. Asian Pac. J. Cancer Prev. *15*, 3471–3476.

30. Yang, L., Song, X., Zhu, J., Li, M., Ji, Y., Wu, F., Chen, Y., Cui, X., Hu, J., Wang, L., et al. (2017). Tumor suppressor microRNA-34a inhibits cell migration and invasion by targeting MMP-2/MMP-9/FNDC3B in esophageal squamous cell carcinoma. Int. J. Oncol. *51*, 378–388.

31. Yao, Z., Yuan, T., Wang, H., Yao, S., Zhao, Y., Liu, Y., Jin, S., Chu, J., Xu, Y., Zhou, W., et al. (2017). MMP-2 together with MMP-9 overexpression correlated with lymph node metastasis and poor prognosis in early gastric carcinoma. Tumour Biol. *39*, 1010428317700411.

32. National Research Council Committee (2011). Guide for the Care and Use of Laboratory Animals, 8th Edition (National Academies Press).

33. Deng, B.H., Yao, Y.S., Hao, W.P., and Wang, J.W. (2002). Primary culture of bladder epithelial cells in vitro. J. Clin. Rehabil. Tissue Engin. Res *16*, 4495–4498.

34. Livak, K.J., and Schmittgen, T.D. (2001). Analysis of relative gene expression data using real-time quantitative PCR and the 2(-Delta Delta C(T)) Method. Methods *25*, 402–408.